Biochimica et Biophysica Acta 1832 (2013) 1105–1116

Contents lists available at SciVerse ScienceDirect

Biochimica et Biophysica Acta

journal homepage: www.elsevier.com/locate/bbadis

V-ATPase is a candidate therapeutic target for Ewing sarcoma

Sofia Avnet [a,*], Gemma Di Pompo [a], Silvia Lemma [a], Manuela Salerno [a], Francesca Perut [a], Gloria Bonuccelli [a], Donatella Granchi [a], Nicoletta Zini [b], Nicola Baldini [a,c]

[a] Laboratory for Orthopaedic Pathophysiology and Regenerative Medicine, Istituto Ortopedico Rizzoli, via di Barbiano 1/10, 40136, Bologna, Italy
[b] IGM-CNR, Unit of Bologna, c/o Istituto Ortopedico Rizzoli, via di Barbiano 1/10, 40136 Bologna, Italy
[c] Department of Biomedical and Neuromotor Sciences, University of Bologna, via di Barbiano 1/10, 40136, Bologna, Italy

ARTICLE INFO

Article history:
Received 19 October 2012
Received in revised form 29 March 2013
Accepted 2 April 2013
Available online 8 April 2013

Keywords:
Ewing sarcoma
Glycolysis
Extracellular acidification
V-ATPase

ABSTRACT

Suppression of oxidative phosphorylation combined with enhanced aerobic glycolysis and the resulting increased generation of protons are common features of several types of cancer. An efficient mechanism to escape cell death resulting from intracellular acidification is proton pump activation. In Ewing sarcoma (ES), although the tumor-associated chimeric gene EWS-FLI1 is known to induce the accumulation of hypoxia-induced transcription factor HIF-1α, derangements in metabolic pathways have been neglected so far as candidate pathogenetic mechanisms. In this paper, we observed that ES cells simultaneously activate mitochondrial respiration and high levels of glycolysis. Moreover, although the most effective detoxification mechanism of proton intracellular storage is lysosomal compartmentalization, ES cells show a poorly represented lysosomal compartment, but a high sensitivity to the anti-lysosomal agent bafilomycin A1, targeting the V-ATPase proton pump. We therefore investigated the role of V-ATPase in the acidification activity of ES cells. ES cells with the highest GAPDH and V-ATPase expression also showed the highest acidification rate. Moreover, the localization of V-ATPase was both on the vacuolar and the plasma membrane of all ES cell lines. The acidic extracellular pH that we reproduced in vitro promoted high invasion ability and clonogenic efficiency. Finally, targeting V-ATPase with siRNA and omeprazole treatments, we obtained a significant selective reduction of tumor cell number. In summary, glycolytic activity and activation of V-ATPase are crucial mechanisms of survival of ES cells and can be considered as promising selective targets for the treatment of this tumor.

1. Introduction

Cancer cells survive and proliferate in competition with somatic cells and according to the physical and biological properties of their microenvironment [1]. During cancer progression, as the tumor mass increases in size, neoplastic cells outgrow their blood supply and lack of adequate access to oxygen and nutrients. It is well documented that tumors induce a program of adaptive responses to thrive under hypoxic conditions by switching their metabolism to upregulated glycolysis and by releasing pro-angiogenic factors [2]. However, according to Otto Warburg's findings [3], tumor cells may continue to metabolize carbon by the glycolytic pathway even under adequate oxygen conditions. Therefore, regardless of hypoxia [4], aerobic glycolysis is a constant feature in cancer development, as suggested by the high levels of glucose consumption detected by positron emission tomography in most malignancies [5]. The high, constant level of glycolytic activity of tumor cells leads to an increased production of lactic acid that decreases the pH of the extracellular microenvironment. Previous authors have demonstrated that the extracellular pH (pHe) of different tumors is in the range of 5.7–7.3 [6–8], whereas the pHe level of normal tissues is significantly more alkaline (7.2–7.5). The existence of an acidic intracellular pH (pHi) is also indicated in vivo by magnetic resonance spectroscopy [9]. To maintain pH homeostasis and escape apoptosis induced by an increase in proton concentration in the cytosol, cancer cells increase the activity and/or expression of several pH regulators, resulting in the alkalinization of pHi and acidification of pHe [10]. Indeed, an increased expression and activity of the transmembrane vacuolar (H^+)-ATPase (V-ATPase) is a constant feature of several tumor types, and its inhibition has been suggested as a promising therapeutic target [11–14]. V-ATPase is an ATP-driven proton pump that acidifies the intracellular compartment and transports protons across the plasma membranes, both in physiological processes and in human diseases [15]. V-ATPase is a large multisubunit complex composed of a peripheral domain (V_1), responsible for hydrolysis of ATP, and an integral domain (V_0) that carries out proton transport [15]. In sarcoma cells, the survival mechanism under acidic conditions and the activity of V-ATPase are still entirely unexplored.

Abbreviations: pHe, extracellular pH; pHi, intracellular pH; V-ATPase, vacuolar (H^+)-ATPase; HIFs, hypoxia-inducible factors; HSP60, heat shock protein 60; GAPDHm, glyceraldehyde-3-phosphate dehydrogenase; OHPHOS, oxidative phosphorylation; BEC, bioenergetic; PAS, periodic acid-Schiff reaction; BF-1, bafilomycin A1; OME, omeprazole

* Corresponding author at: Laboratory for Orthopaedic Pathophysiology and Regenerative Medicine, Istituto Ortopedico Rizzoli, via di Barbiano 1/10, 40136 Bologna, Italy. Tel./fax: +39 0516366897.
E-mail address: sofia.avnet@ior.it (S. Avnet).

0925-4439/$ – see front matter © 2013 Elsevier B.V. All rights reserved.
http://dx.doi.org/10.1016/j.bbadis.2013.04.003

In this paper, we focused on Ewing sarcoma (ES), a rapidly growing, highly malignant bone tumor developing metastases in the vast majority of patients unless multiagent chemotherapy is applied [16]. ES is the second most frequent bone tumor in childhood and adolescence, and is characterized by the presence of EWS–ETS gene rearrangements [17]. Recently, some authors have reported that, in ES, hypoxia enhances the malignant phenotype through an upregulation of the EWS–FLI1 fusion gene by hypoxia-inducible factor (HIF)-1α [18]. HIF-1α and HIF-1β are the main mediators of the hypoxic response that favors cell proliferation through the control of the expression of numerous genes that regulate glucose uptake, metabolic reprogramming from oxidative phosphorylation (OXPHOS) to glycolysis, and lactic acid production [19,20]. Interestingly, glycogen granules accumulate in normal or cancer cells in a HIF-1-dependent manner [21], and the positive glycogen reaction to the cytochemical periodic acid-Schiff (PAS) stain is an additional feature that is currently used for the diagnosis of ES in parallel to the molecular detection of the EWS-FLI1 fusion gene [22].

In this study, we endorsed V-ATPase as a survival mechanism of ES cells under acidic conditions, and as a promising selective therapeutic target to be considered for future trials.

2. Material and methods

2.1. Cell lines

A-673, SK-N-MC, RD-ES, SK-ES-1 ES cell lines were purchased from the American Type Culture Collection (ATCC, Manassas, VA), and cultured in RPMI (Sigma, Manassas, VA) buffered at 7.4 pH plus 20 units/mL penicillin, 100 μg/mL streptomycin (Gibco, Life Technologies, Paisley, UK), 10% fetal bovine serum FCS (FCS, Euroclone, Milan, Italy) (complete medium). Normal human fibroblasts (hFG) were isolated from the gingiva of healthy donors. Tissue explants were cultured in complete medium [23]. All the cell cultures were incubated at 37 °C in a humidified 5% CO_2 atmosphere. In the different assays complete medium was also used at different pH (5.8 or 6.5). The specific pH in the culture medium was maintained by using different concentrations of sodium bicarbonate needed for the preset pH in 5% CO_2 atmosphere, according to the Henderson–Hasselbach equation. At the end-point of each experiment, the final pH in the supernatant was always measured to ascertain the maintenance of the pH value along the incubation time. For all assays but the bone invasion assay, cells were cultured on human fibronectin (Gibco, Life Technologies).

2.2. Western blotting

Western blotting was carried out to detect ATP synthase subunit α, Complex II subunit 30 kDa, Complex III subunit Core 2, heat shock protein 60 (HSP60), glyceraldehyde-3-phosphate dehydrogenase (GAPDH), V_0c and V_1B2 subunits of the V-ATPase protein, and actin in total lysates. Cells were maintained in complete medium and lysated at semi-confluence with RIPA buffer [Tris pH 7.6 50 mM, NaCl 150 mM, Triton-X 100 5%, sodium deoxycholate 0.25%, EGTA pH 8 1 mM, NaF 1 mM] (Sigma) supplemented with protease inhibitors (Roche, Milan, Italy). Equal amounts of protein lysates were subjected to reducing SDS-PAGE on a polyacrylamide gel, transferred to nitrocellulose membranes, and subjected to immunoblot analysis. Blots were probed with MitoProfile Total OXPHOS human antibody Cocktail 1:300 (Abcam, Cambridge, UK), or with an anti-GAPDH (1:2000, Santa Cruz Biotechnology, Dallas, TX), anti-HSP60 (1:2000, Sigma), anti-V_1B2 V-ATPase (1:200, Sigma), anti-V_0c V-ATPase (1:50, Abcam), anti-actin (1:1000, Cell Signaling, Danvers, MA) polyclonal antibodies. Incubation with horseradish peroxidase-conjugated anti-rabbit, anti-mouse (GE Healthcare, Buckinghamshire, UK), or anti-goat antibodies (Santa Cruz Biotechnology, Dallas, TX) followed. To detect different antigens within the same blot, nitrocellulose membranes were stripped with Restore Western Blot Stripping buffer (Thermo Fisher Scientific, Rockford, IL), and then reprobed. The reaction was revealed by a chemiluminescence substrate (ECL Western Blotting Detection Reagents, GE Healthcare, Chalfont St. Giles, Buckinghamshire, UK). Immunoblot assays were repeated five times for the BEC index assay and three times for all the other assays. Signal from each band was quantified by dedicated software for densitometric evaluation (Quantity One, Biorad Laboratories Headquarters, Hercules, CA).

2.3. Mitochondrial activity

To stain mitochondria, rhodamine-based MitoTracker Orange CMTMRos (Molecular Probes, Life Technologies) was used. MitoTracker stains live mitochondria with an intact membrane potential. Briefly, cells were incubated with MitoTracker diluted in serum free RPMI to a final concentration of 250 nM for 10–15 min at 37 °C. Then, cells were fixed with 3% paraformaldehyde and 300 mM sucrose (Sigma) in PBS. Analysis of labeled cells was performed using a confocal microscope (Nikon D-Eclipse C-1, Tokyo, Japan).

2.4. Immunofluorescence

For the immunofluorescence staining with an antibody against the surface of intact mitochondria, cells were washed with PBS, fixed in 3% paraformaldehyde in PBS containing 300 mM sucrose for 20 min at 22 °C. After washing in PBS, permeabilization was performed with 0.1% Triton X-100 for 5 min. Then, cells were incubated with the MAB1273 antibody 1:100 (Millipore, Billerica, MA), and subsequently with anti-mouse Alexa green 488 nm (Molecular Probes, Life Technologies), and observed by confocal microscopy. For the co-localization analysis of LC3B or V-ATPase V_0a1 with lysosomes, before washing and fixation, living cells were incubated with Lysotraker (0.25 μM, Molecular Probes, Life Technologies) in complete medium for 30 min at 37 °C. After the incubation with the primary antibody (anti-V-ATPase V_0a1 antibodies 1:30, Sigma, and anti-LC3B antibody 1:50, Cell Signaling), and secondary anti-mouse antibody Alexa green 488 nm (1:1000, Molecular Probes, Life Technologies), nuclei were stained with Hoechst 33258 (1.25 μg/ml Sigma). Cells were then analyzed by a confocal microscope (Nikon TI-E). For the co-localization analysis of V-ATPase V0a1 with plasma membrane, cells were washed and fixed as described above, but not permeabilized. After the immunofluorescence stain for the ATPase V_0a1, cells were also stained with a Fluorescent Cell Linker Dye (PKH26, Sigma) with long aliphatic tails that bind lipid regions of the cell membrane.

2.5. Lysosome staining

Living adherent cells at low confluence and maintained in complete medium were treated with 0.37% neutral red (Sigma) for 2 h at 37 °C and 5% CO_2, washed with PBS, and observed. Alternatively, for fluorescence experiments, cells were incubated with 1 μg/ml acridine orange dye (Sigma) for 10 min at room temperature in complete medium in the dark, and rinsed with PBS prior to fluorescence microscopy analysis.

2.6. Electron microscopy

For ultrastructural evaluation, pellets of ES cells were fixed in 2.5% glutaraldehyde in 0.1 M cacodylate buffer (Sigma), pH 7.4, for 1 h at RT, postfixed with 1% osmium tetroxide (Sigma), dehydrated in a graded series of ethanol, and embedded in Epon. Thin sections were stained with uranyl acetate and lead citrate, and observed with a transmission electron microscope (Zeiss, Milan, Italy).

2.7. Growth assay

a) *Indirect assay*: Cells were seeded in 96-well plates (10,000 cells/well for hFG and 50,000 cells/well for ES cells) in complete medium. After 24 h, the medium was changed with complete medium at pH 6.5 or pH 7.4, added or not with bafilomycin A1 (BF-1) 2–5–10 nM (Sigma), or with omeprazole (OME) 60–120–210 μM (Sigma). After additional 72 h, the cell number was evaluated by an acid phosphatase assay, as previously described [24]. Briefly, the culture medium was removed and each well was washed once with PBS, and added with 100 μl of buffer containing 0.1 M sodium acetate (pH 5.0), 0.1% Triton X-100, and 5 mM p-nitrophenil phosphate. The plate was placed in a 37 °C incubator for 3 h. The reaction was stopped with the addition of 10 μl of a 1 N NaOH, and color development was assayed at 405 nm using a microplate reader (Tecan Infinite F200pro, Männedorf, Switzerland); b) *Direct assay*: Cells were seeded in 6-well plates (50,000 cells/well for hFG and 150,000 cells/well for ES cells) in complete medium. After 24 h, the medium was changed with new complete medium at pH 6.5 added or not with BF-1 10 nM (Sigma), or OME 120 and 210 μM (Sigma). Cell growth was evaluated after additional 72 h by the direct counting of cells using erythrosine dye (Sigma). The experiments were repeated three times, and with two replicate for each assay.

2.8. Extracellular pH measurement

Cells were seeded into 75 cm^2 flasks (133,000 cells/cm^2). As a control, flasks with medium alone were also set. After 24 h at 37 °C in a humidified 5% CO_2 atmosphere, when cells reached the semi-confluence, flasks with or without cells were washed twice with PBS, and supplemented with 10 ml of RPMI without sodium bicarbonate, and with 0.1% FCS. The flasks were sealed in order to avoid gas exchange with the external microenvironment. After additional 24 h, flasks were opened, the medium collected, and the pH promptly measured by a digital pH-meter (pH 301, HANNA Instruments, Milan, Italy). The difference of the pH value of the collected medium vs control was reported as pHe decrement. The experiment was repeated three times, with two replicate for each assay.

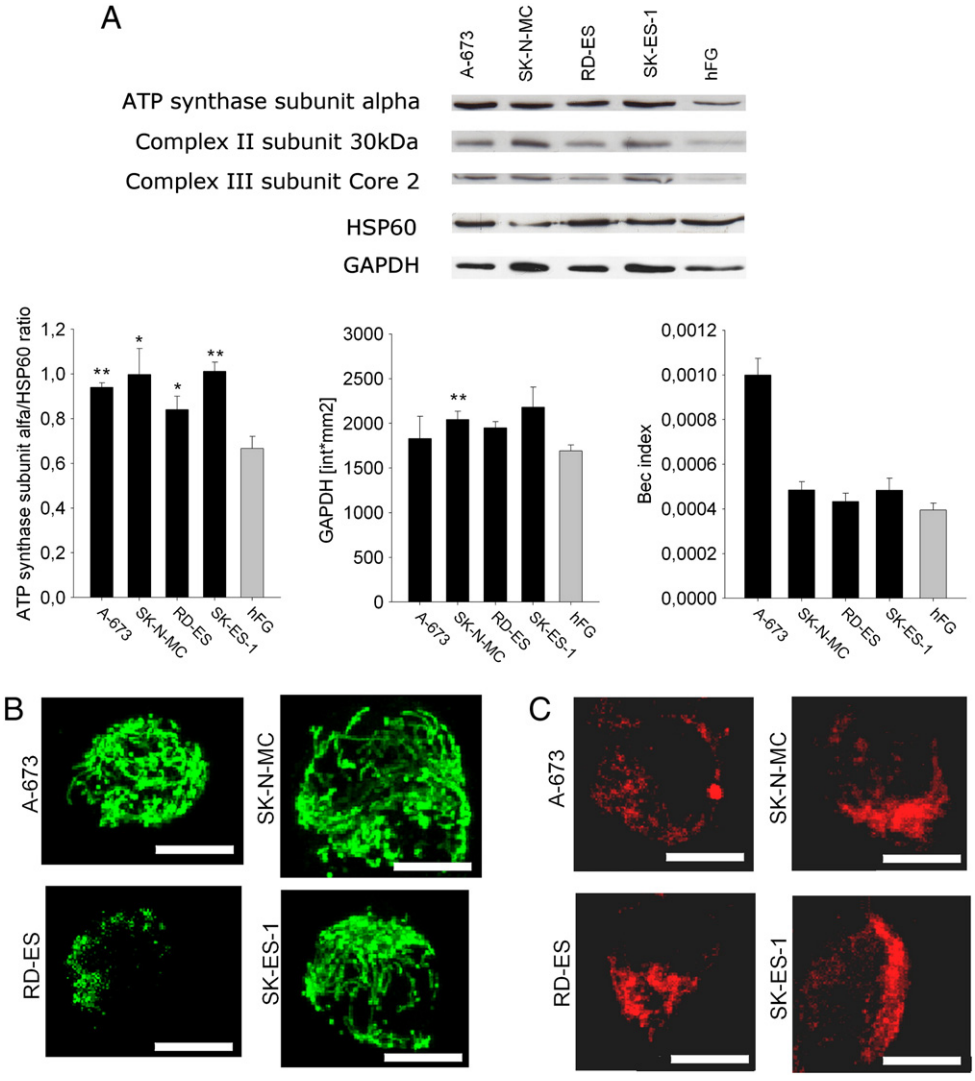

Fig. 1. Ewing sarcoma bioenergetic signature. The ES cell lines were studied for mitochondrial and glycolytic activity by analyzing the BEC index and Mytotraker staining, and compared to normal human fibroblasts (hFG). (A) Upper panel: Western blot analysis of the ATP synthase subunit α, Complex II subunit 30 kDa, Complex III subunit Core 2, HSP60, and GAPDH. Lower panel: densitometric analysis of Western blot (n = 3, $^*P < 0.05$). The Ratio ATP synthase subunit/alpha/HSP60/GAPDH was referred as the BEC index. (B) Mitochondrial mass analyzed by immunofluorescence using an anti-mitochondria surface-FITC antibody and (C) MytoTracker Orange CMTMRos staining, observed by confocal microscope. Representative overlayered images of 35 xy fields of 0.5 μm distance, scale bar 10 μm. ES cells have both higher mitochondrial and glycolytic activity.

2.9. Apoptosis analysis

In order to assess if acidic pHe (6.5) can induce apoptosis, ES cells were seeded on glass slides at low density and in complete medium. After 24 h, the medium was changed with complete medium at pH 6.5, or 7.4 with or without staurosporine (100 μM, Sigma) as a positive control. After 4 days, cells were fixed and permeabilized as described above, and incubated for 30 min with Hoechst 33258 (2.25 μg/ml,

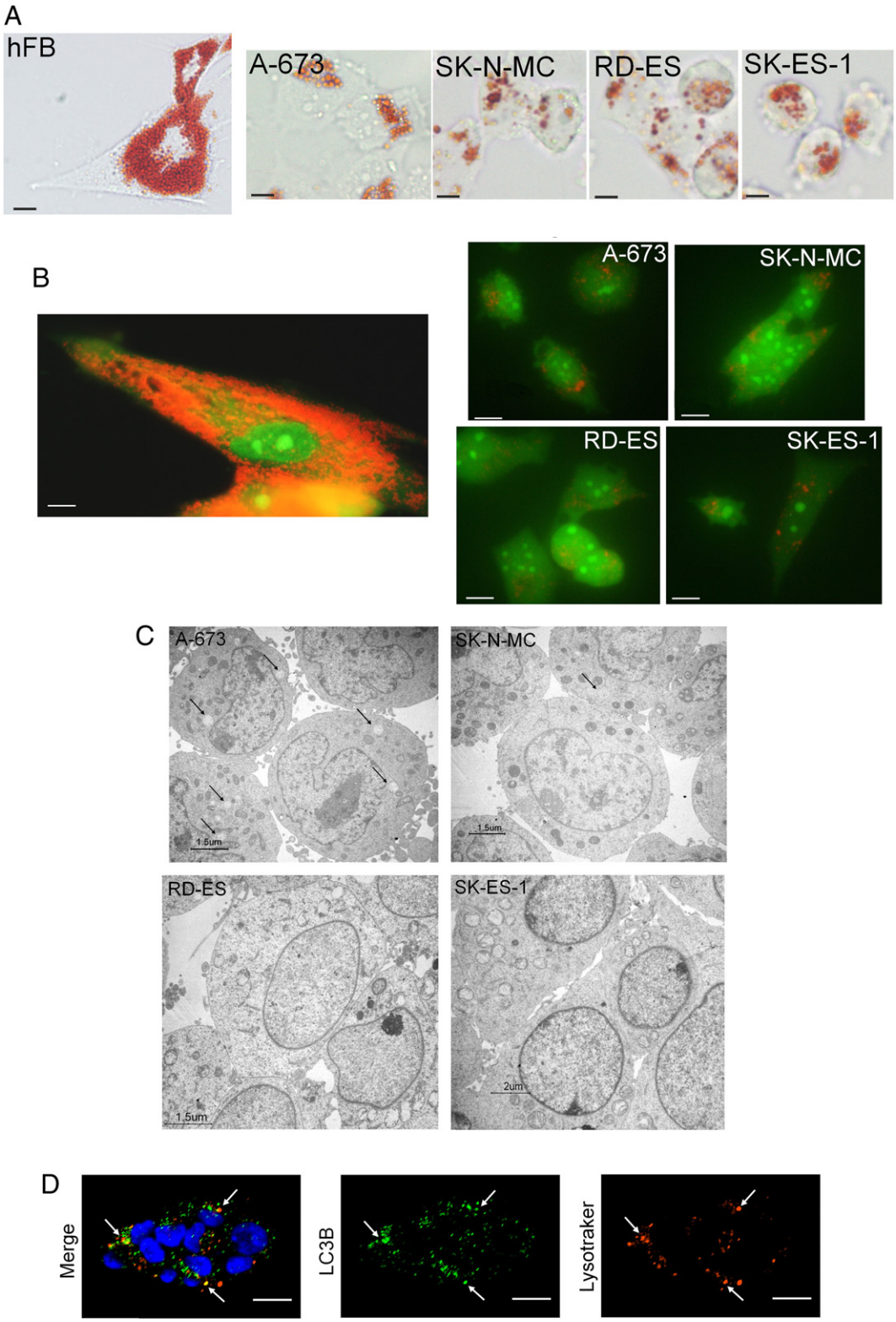

Fig. 2. Lysosome compartment of Ewing sarcoma cells. (A) Neutral red and (B) Acridine orange staining, representative images. Red staining is associated with lysosome compartment. Scale bar 10 μm. (C) Ultrastructural morphology. Black arrows, lysosomes. Representative images, scale bar 1.5 μm. (D). LC3B immunofluorescence (green) and Lysotracker staining (red) of A-673 cells. Nuclei are counterstained with Hoechst 333258 (blue). Representative image of an xy field acquired by confocal microscope. White arrows, co-localization of LC3B and lysosome staining. Scale bar 20 μm. ES cells have a lower number of lysosomes when compared to hFG.

Sigma). The percentage of cells with apoptotic bodies out of a total of 100 cells, and in 3 different fields, was counted using an epifluorescent microscope. The experiment was repeated three times.

2.10. Cell cycle analysis

In order to analyze cell cycle distribution after exposure to acidic conditions, DNA content and bromodeoxyuridine (BrdU) incorporation were determined by simultaneous analysis of propidium iodide and fluorescein isothiocyanate (FITC)-conjugated anti-BrdU fluorescence. Cells were seeded at low density in complete medium, and after 24 h the medium was changed with complete medium at pH 6.5 or 7.4. After additional 48 h, cells were incubated with 10 mM BrdU (Sigma) for 60 min before harvesting. Cells were collected by trypsinization, followed by fixation in 40% ethanol for 20 min. Partial DNA denaturation was performed by incubating cells in HCl, followed by neutralization with sodium tetraborate. Samples were then exposed to a monoclonal anti-BrdU FITC antibody (BD Biosciences, Erembodegem, Belgium), washed, and finally stained with 2.5 mg/ml propidium iodide (Sigma). Flow cytometric analysis was performed with a Coulter EPICS1 XL Flow Cytometer (Coulter Corporation, Beckman Coulter, Milan, Italy). Monoparametric and biparametric analyses were performed using the WinMDI 2.7 software. The experiment was repeated three times.

2.11. Invasion assays

a) *Gelatin quenching*: metalloproteinase activity was quantified by seeding ES cells in complete medium in 24 well plates (350,000 cells/well). After 24 h, medium was changed with complete medium at pH 5.8–6.5–7.4. After additional 48 h, cells were washed once with PBS, and incubated at 37 °C with 500 μl of PBS for 1 h. PBS was then collected, centrifuged and the supernatant was used for the gelatin quenching assay. Adherent cells were lysated with RIPA buffer with protease inhibitors as previously described. Equal amounts of proteins from the supernatant were added to 100 μl of gelatin quenching (DQ™ Gelatin, Invitrogen, Life Technologies) in a 96 well plate. After 24 h at 37 °C, the fluorescence emission was measured by a microplate reader. Results from samples were subtracted by results obtained with the acellular condition, and normalized by dividing for the total protein content in the cell lysates. The experiments was performed in duplicate and repeated three times. b) *Bone invasion*: to measure the bone resorption ability, ES cells were seeded (10,000) onto 96-well plates coated with europium-conjugated Type I collagen (Osteolyse Assay Kit, Cambrex, East Rutherford, NJ) in complete medium, and incubated at 37 °C in a humidified 5% CO_2 atmosphere. Wells with medium without cells were also set. After one day, the medium was changed at different pH (6.5 or 7.4). After 2 days of culture, supernatants were transferred into new wells containing the fluorophore releasing reagent. Fluorescence emission was determined by a time-resolved plate reader (Wallac Victor; Perkin Elmer, Waltham, MA). The RFU values of the supernatant from different ES cultures were then subtracted with supernatant from acellular wells with the medium at the respective pH.

2.12. Clonogenic assay

Clonogenic efficiency was determined by seeding ES cells at low density (280 cells in 60 mm diameter Petri dishes) in complete medium, and incubated at 37 °C in a humidified 5% CO_2 atmosphere. After 24 h, medium was changed with complete medium at different pH (6.5 or 7.4). Colonies were fixed with methanol, stained with crystal violet, and counted after 6–7 days. The experiment was repeated four times, with two replicate for each assay.

2.13. Real-time PCR

Total RNA was extracted from semi-confluent cells using the RNeasy Mini Kit (Qiagen, Hilden, Germany). Total mRNA was reverse transcribed by Advantage RT-for-PCR Kit (Roche). The expression of V-ATPase V_0c

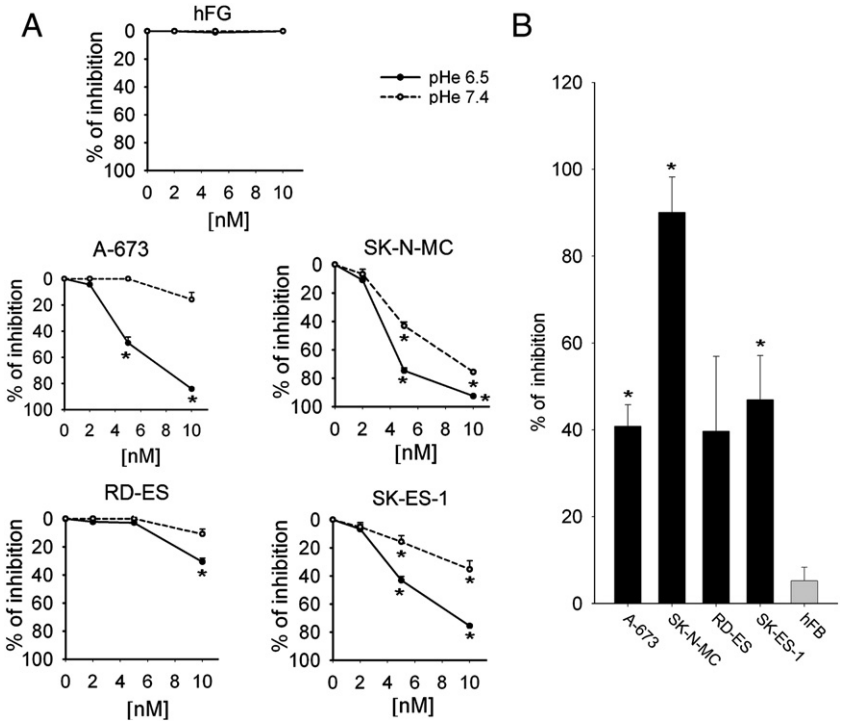

Fig. 3. Effect of bafilomycin A1 on cell number of Ewing sarcoma. (A) Acid phosphatase indirect assay of cells treated at different concentration of bafilomycin A1 (BF-1) at different pH after 72 h. Percentage of inhibition with respect to untreated cells at the respective pH (mean ± SE, n = 4, $^*P < 0.05$). (B) Percentages of inhibition at 72 h of the number of cells treated with BF-1 (10 nM) at pH 6.5 with respect to untreated cells (mean ± SE, n = 4, $^*P < 0.05$). BF-1 significantly impaired ES cell number and with more efficacy under acidic condition, whereas hFG were completely unaffected.

(NM_001694.2) was evaluated by Real Time PCR by using a Light Cycler instrumentation (Roche), by amplifying 1 μg of cDNA and the Universal Probe Library System (Roche). Probes and primers were selected using a web-based assay design software (ProbeFinder https://www.roche-applied-science.com). V-ATPase V_0c-f 5′-TTCGTTTTTCGCCGTCAT-3′; V-ATPase V_0c-r 5′-CCACTGGGATGATGGACTTC-3′. The protocol of amplification was: 95 °C for 10 min; 95 °C for 10 s, 60 °C for 30 s, and 72 °C for 1 s for 45 cycles; 40 °C for 30 s. Results were expressed as the ratio

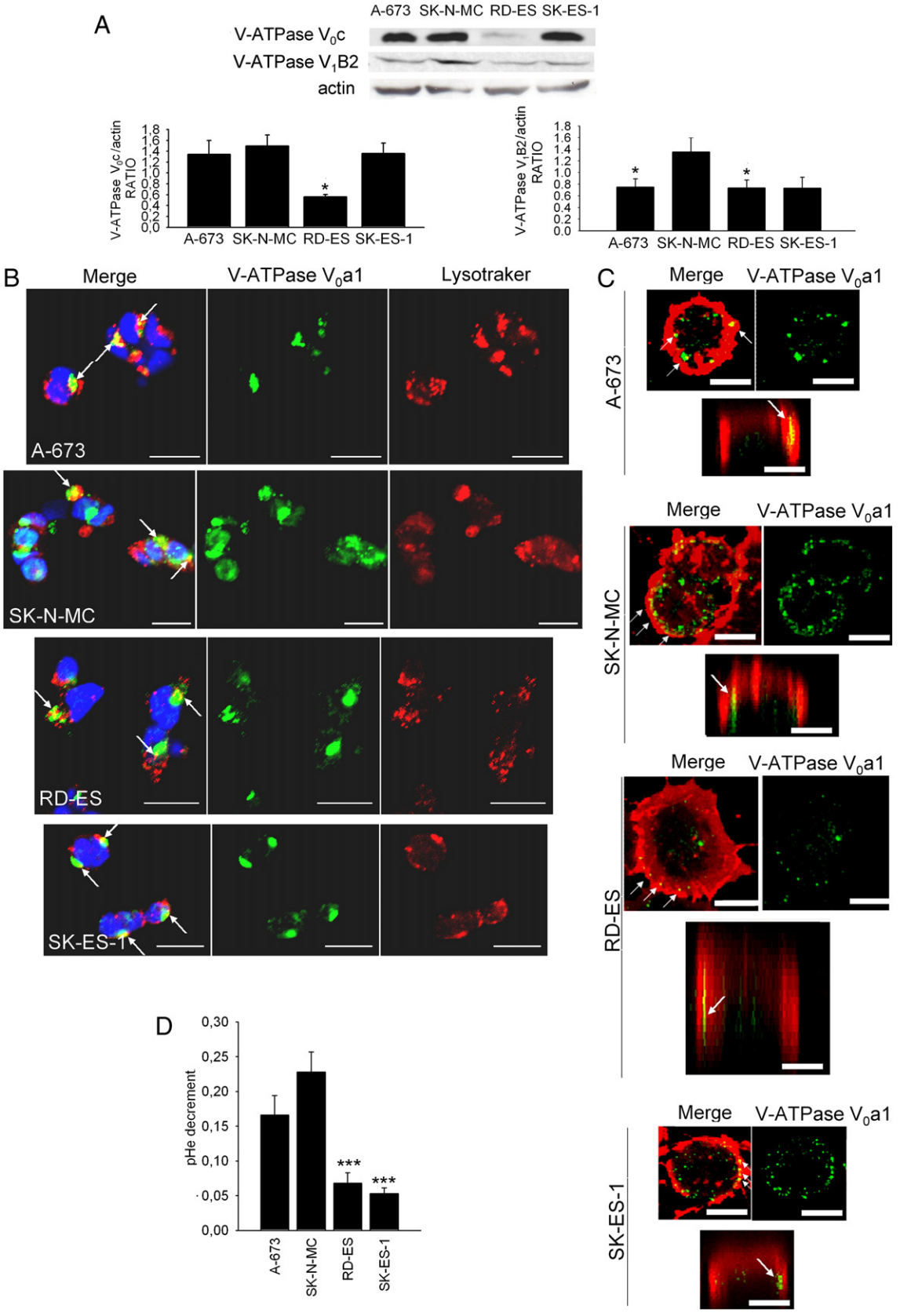

between V0c subunit and β-actin as a reference gene (NM_001101.2; ACTB-f 5′-CCAACCGCGAGAAGATGA-3′; ACTB-r 5′-CCAGAGGCGTACA GGGATAG-3′) according to the $2^{-\Delta\Delta CT}$ method [25]. The experiment was repeated two times, with two replicates for each assay.

2.14. siRNA transfection

Specific gene silencing effect was obtained by siRNA technology associated with pipette-type electroporation. SK-N-MC and A-673 cells were trypsinized at semi-confluence, and counted after erythrosine dye staining. 15 μL of cell suspension containing 300,000 cells and 2 pmol of specific siRNA (ON-TARGETplus Human ATP6V0C siRNA Smart poll, Dharmacon, Thermo Scientific, Waltham, MA) or control siRNA (siRNA ctr, ON-TARGETplus Non-targeting Control Pool, Dharmacon) were transferred into a 1-mm cuvette (Neon® Transfection System, Invitrogen, Life Technologies). Electroporated cells were transferred into 2 mL of complete medium, and seeded in 12-well plates (30,000 cells/well) for RNA isolation and cell counting or in a plate of 10 cm of diameter for protein extraction (600,000 cells). After one day (T0), medium was changed with complete medium at pH 6.5. At T0 and after additional 3 days (T1) cells were counted by using erythrosine dye. At T1, cells were also used to isolate RNA and protein, as previously described. Both assays were repeated three times in duplicate.

2.15. Statistical analysis

Statistics was performed with the StatViewTM 5.0.1 software (SAS Institute, Cary, NC). Due to the low number of observations, data were considered as not normally distributed, and nonparametric tests were used. The Mann-Whitney U test was used for the difference between groups. In all statistical calculations, data were expressed as mean ±SE, and differences were considered significant at P values ≤ 0.05.

3. Results

3.1. Glycolytic metabolism in Ewing sarcoma cells

The glycolytic activity and the mitochondrial respiration of ES cells were evaluated in comparison with that of hFG by Western blot analysis, to define the bioenergetic cellular (BEC) index, and by MytoTracker staining. The BEC index (β-F1-ATPase/HSP60/GAPDH ratio) describes the bioenergetic activity of mitochondria relative to the glycolytic potential of the cell [26,27]. In comparison to hFG, ES cells showed a significantly higher mitochondrial activity and an increased glycolytic activity (Fig. 1A). The MitoTracker staining co-localizes with cytochrome c [28], and enters only into mitochondria with a normal membrane potential and function. MitoTracker staining is therefore an indirect marker of OXPHOS of healthy and functional mitochondria. By using both MitoTracker and FITC staining with an antibody against an antigen of intact mitochondrial surface, we confirmed the presence of a high number of active mitochondria in ES cells (Fig. 1B and C). In conclusion, ES cells showed a higher glycolytic activity, although associated with a higher OXPHOS, as compared to hFG.

3.2. Lysosomes in Ewing sarcoma cells

To evaluate if the higher glycolytic activity of ES cells correspond to an increase in lysosome number, we used neutral red and acridine orange staining. In comparison to normal hFG, ES cells showed a lower number of lysosomes (Fig. 2A and B), as also confirmed by ultrastructural analysis (Fig. 2C). By electron microscopy, lysosomes of ES cells appeared to be either multivesicular bodies or secondary lysosomes (data not shown). Part of the observed lysosomes were autolysosomes, as suggested by the positive immunostaining with the autophagy-associated LC3B antigen (Fig. 2D).

To evaluate the role of the lysosomal compartment in ES cells under acidic conditions, we used an indirect assay with increasing concentrations of the anti-lysosomal BF-1 agent at acidic (pH 6.5) versus alkaline standard conditions (pH 7.4). We observed a dose-dependent and significant inhibition of ES cell survival that was further enhanced under acidic conditions (Fig. 3A). Conversely, even the highest concentrations of BF1 were completely ineffective in hFG, either at acidic or alkaline conditions (Fig. 3A). Results obtained in acidic medium were also confirmed by direct cell counting (Fig. 3B). From our results we can assume that, although ES cells show a low number of lysosomes, the anti-lysosome BF1 agent is very effective and selective to impair tumor survival under acidic conditions.

3.3. V-ATPase expression and localization in Ewing sarcoma cells

Since V-ATPase is a key effector of proton secretion and lysosome activity, we analyzed V-ATPase expression and localization in ES cells. The presence of V-ATPase in the cell lysate was verified by using an antibody against the V_0c and V_1B2 subunits in Western blotting analysis (Fig. 4A). In particular, we choose the V_0c as it has been successfully targeted by siRNA strategies also in other cancers [13,29,30], and since it is the target of BF-1 [31]. V-ATPase is formed by two different domains, the V_1 domain and the intramembrane V_0 domain, that can be reversibly dissociated [15], and the expression pattern of a subunit of the V_c domain should be similar to the expression pattern of a subunit of the V_1 domain. The analysis of V_1B2 subunit is a further validation of results obtained on V_0c subunit. All ES cells expressed the V_0c and V_1B2 subunits, and the SK-N-MC cell line at a significantly higher extent. For the immunofluorescence assay, we used an antibody that can stain also non permeabilized cells and recognizes the V_0a1 transmembrane domain. In permeabilized cells, the V_0a1 subunit is localized in the Golgi apparatus in the perinuclear region and in some vesicles and is partially co-localized with lysosome specific staining (Fig. 4B). Adversely, in ES cells with an intact membrane, V-ATPase co-localized with a cell membrane dye (Fig. 4C). Notably, we also found that the ES cell line with the highest expression of V-ATPase, SK-N-MC, also showed the highest acidification activity (Fig. 4D). In summary, in ES cells the V-ATPase is localized in the Golgi apparatus, at the lysosomal compartment, and on the plasmalemma. The most acidifying ES cells also show the highest levels of V-ATPase expression.

3.4. Effects of acidic pHe on Ewing sarcoma cells

As a consequence of a high glycolytic activity, acidification of the microenvironment can strongly modulate key aspects of tumor biology. By

Fig. 4. V-ATPase expression and localization in Ewing sarcoma cells. (A) Western blotting of V_0c and V1B2 subunits of V-ATPase (representative images, upper panel), and densitometric analysis (lower panel, mean ± SE, n = 3, $^*P < 0.05$ vs SK-N-MC). (B) Immunofluorescence of V-ATPase V_0a1 subunit (green) in permeabilized cells incubated with Lysotraker (red) by confocal microscope analysis. Nuclei were counterstained with Hoechst 333258 (blue). White arrows, co-localization of V-ATPase V_0a1 and Lysotraker. Representative images of an xy field, scale bar 20 μm. (C) Immunofluorescence of the transmembrane V-ATPase V_0a1 subunit (green) in not permeabilized cells stained with a cytosolic membrane dye (PKE26, red) by confocal microscope analysis. Representative overlayered images of 35 xy fields of 0.5 μm distance, scale bar 10 μm, merge and green emission images. Z-sections of one chosen scanned XY-section are also shown in the lower panel (XZ-section). White arrows, co-localization. (D) Acidification activity. pH decrement of the unbuffered medium was measured with respect to acellular condition (mean ± SE, n = 6, $0.01 < {}^*P < 0.05$, $0.005 < {}^{**}P \leq 0.01$ vs SK-N-MC). V-ATPase is expressed in all ES cells and localized also at the cell membrane. SK-N-MC cells showed the highest expression of V-ATPase and the highest acidification rate.

maintaining ES cells at an acidic pHe (6.5) we observed that the number of cells was reduced (Fig. 5A), although the number of apoptotic cells was unaffected (Fig. 5B). The lower number of cells at pH 6.5 is possibly a consequence of an increase in the G0-G1 phase of the cell cycle, combined with a decrease of the S phase, as observed in all ES cell lines (Fig. 5C) but RD-ES cells (Fig. 5A). Likewise, the metalloproteinase activity (Fig. 5D) and bone collagen degradation (Fig. 5E) were significantly improved at acidic conditions for almost all the ES cell lines, as

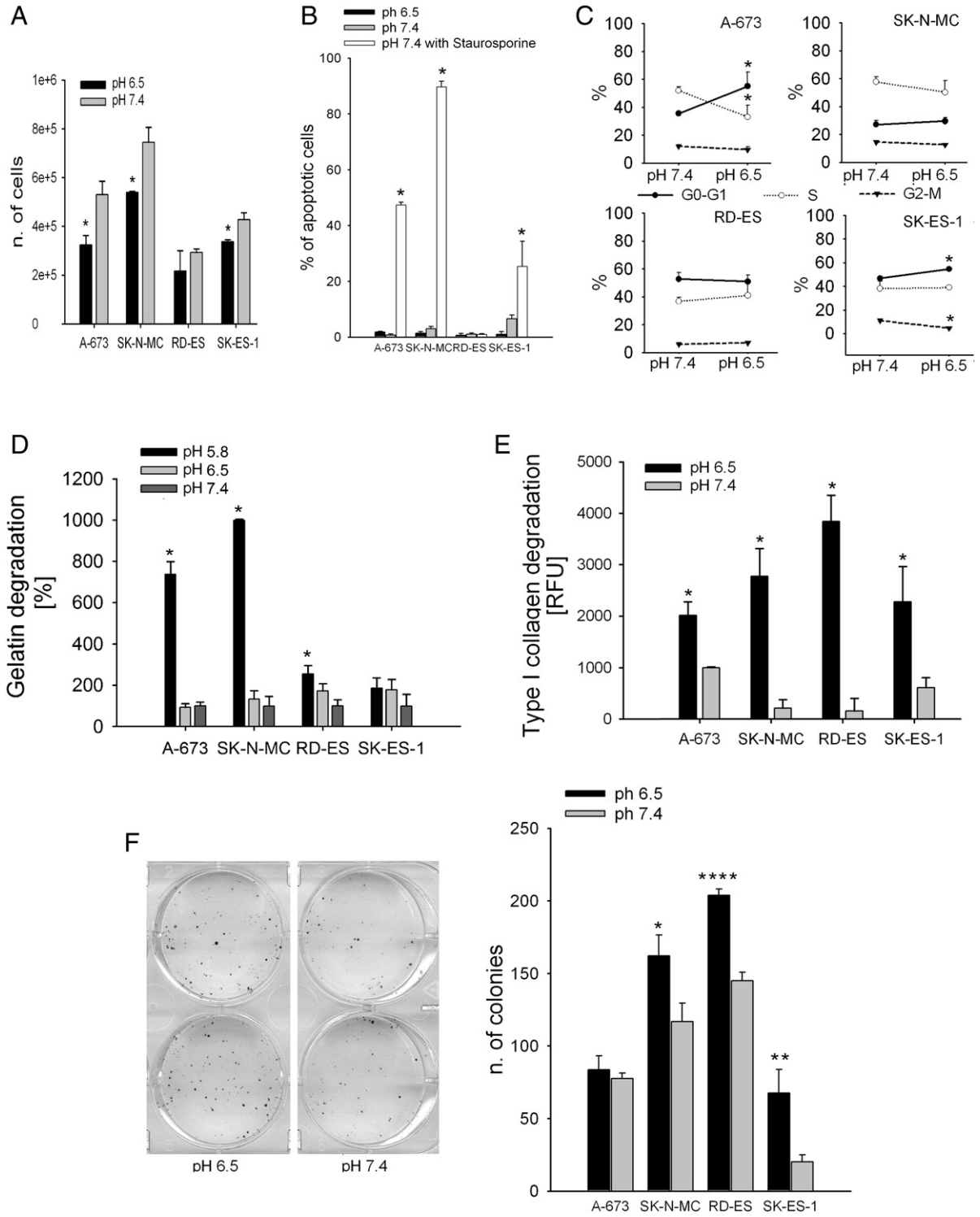

Fig. 5. Effect of acidic pHe on Ewing sarcoma cell number, invasion, and clonogenic efficiency. (A) No. of cells at different pHe at 72 h (mean ± SE, n = 4, $^{*}P < 0.05$ vs pH 7.4). (B) Percentage of apoptotic cells at different pHe. Treatment with staurosporine (100 μM) was used as positive control (mean ± SE, n = 3, $^{*}P < 0.05$). (C) Cell cycle analysis with anti-BrdU antibody and cytofluorimetric analysis at different pH (mean ± SE, n = 3, $^{*}P < 0.05$ vs pH 7.4). (C) Gelatin degradation activity of cell supernatant at different pH. Results are reported as the percentage of fluorescence emission with respect to acellular supernatant (mean ± SE, n = 3, $^{*}P < 0.05$). (D) Type I collagen degradation of cells at different pHe, measured by Osteolyse assay kit (mean ± SE, n = 3, $^{*}P < 0.05$). (E) Number of colonies formed under different pHe of ES cells seeded at low density (left panel, representative images for SK-N-MC cells; right panel, mean ± SE, n = 8, $0.01 < {}^{*}P < 0.05$, $0.005 < {}^{**}P \leq 0.01$, $^{****}P < 0.001$). At acidic pHe ES cells showed a lower growth rate but a higher is invasion ability and clonogenic efficiency.

compared to the pHe 7.4 condition. Interestingly, the acidic microenvironment also significantly increased the clonogenic efficiency of ES cells (Fig. 5F). We can therefore postulate that, although the acidic microenvironment decreases the proliferation rate of ES cells, it prompts tumor cell to a more aggressive phenotype.

3.5. Effect of V-ATPase inhibition on tumor growth of Ewing sarcoma

First, we demonstrated the specific and significant inhibition of mRNA and protein expression in SK-N-MC and A-673 cells treated with a siRNA against the V_0c subunit of V-ATPase (Fig. 6A). Afterwards,

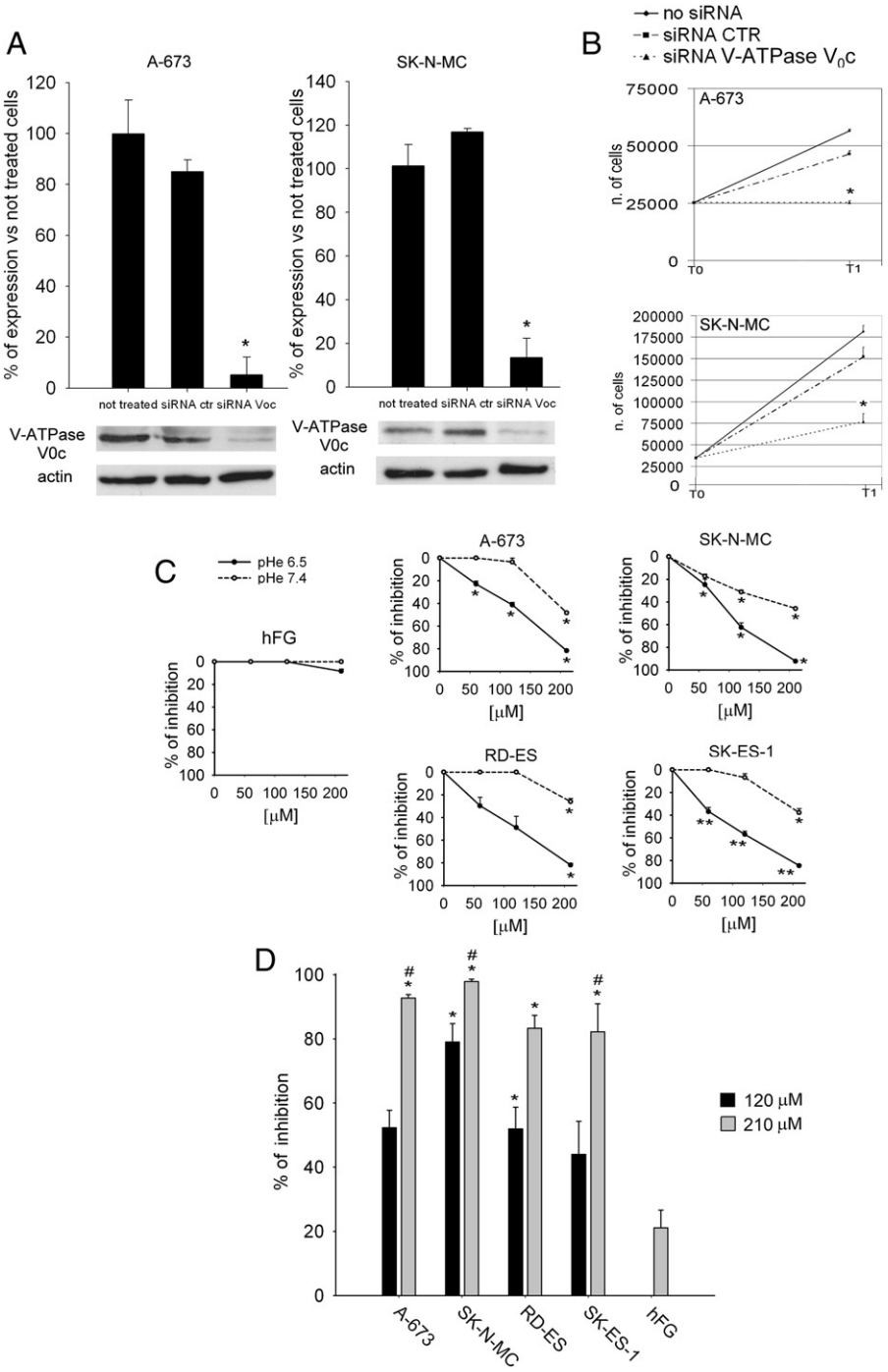

Fig. 6. Effect of V-ATPase blockage on cell growth of Ewing sarcoma. (A) Upper panel, graph representation of mRNA analysis of SK-N-MC and A-673 cells electroporated with a siRNA against the V-ATPase V_0c subunit. Results are reported as the percentage of expression in respect with the not treated condition (mean ± SE, n = 3, $^*P < 0.05$). Lower panel, western blot analysis of the protein expression of V-ATPase V_0c subunit in electroporated cells, representative images. (B) Number of SK-N-MC and A-673 cells electroporated with the V-ATPase V_0c siRNA and maintained at 6.5 pH over time (T1 = 72 h) (mean ± SE, n = 6, $^*P < 0.05$). (C) Acid phosphatase indirect assay of cells treated with omeprazole at different pH and at different concentrations, after 72 h. Results are reported as the percentage of inhibition with respect to untreated cells at the respective pH (mean ± SE, n = 4, $0.01 < {}^*P < 0.05$, $0.005 < {}^{**}P \leq 0.01$). (D) Percentages of inhibition at 72 h of the number of cells treated with omeprazole (120–210 μM) at pH 6.5 with respect to untreated cells (mean ± SE, n = 4, $^*P < 0.05$ vs untreated cells). Omeprazole at 210 μM was also significantly more effective than 120 μM ($^{\#}P < 0.05$). Either specific siRNA, or omeprazole were significantly effective to inhibit ES cell number. Omeprazole significantly impaired ES cell number and with more efficacy under acidic condition, whereas hFG were completely unaffected.

we showed that treatment with V-ATPase V_0c siRNA significantly decreased the number of cells of both SK-N-MC and A-673 cells at acidic pHe (pHe 6.5, Fig. 6B, 57.6 ± 4.9% of inhibition for SK-N-MC $P = 0.0209$, and 55.2 ± 7.0% for A-673 $P = 0.0339$ vs no siRNA). Similarly, by using an indirect assay, we obtained a strong inhibition of cell number for all the ES cells treated both at acidic (pH 6.5) and alkaline (pH 7.4) conditions with the highest dose of the specific anti-V-ATPase agent OME (Fig. 6C). Notably, the inhibition induced by OME was significant also at the lowest concentration, but only at pH 6.5, in all ES cells, with the exception of the RD-ES cell line that also had a low V-ATPase expression (Fig. 4A). Adversely, OME was completely ineffective in hFG (Fig. 6C). Results obtained with OME were further validated by direct cell counting (Fig. 6D). Also in this case, we observed a dose-dependent effect. The most susceptible cell line was SK-N-MC. In summary, inhibition of V-ATPase is dependent on the level of expression of the V-ATPase protein and is an effective strategy to impair ES survival under acidic conditions.

4. Discussion

The role of mitochondria in cancer development and progression is a fundamental and complex issue [32,33]. Since Warburg's theory [3], it is now widely accepted that tumor cells drive a metabolic shift characterized by the suppression of OXPHOS combined with the activation of glycolysis as the main pathway for ATP synthesis [34]. In this study, we verified this metabolic alteration in ES, an extremely aggressive, poorly differentiated cancer of putative mesenchymal origin. According to the bioenergetic signature (BEC index) [26,27], and to the staining with the Mytotraker dye, we found that ES cells have a significantly higher mitochondrial activity with respect to normal fibroblasts. ES cells also showed a higher GAPDH expression, with particular regard to the SK-N-MC cells, reflecting a higher glycolytic activity. In keeping with the in vitro high glucose consumption of ES cells, the sensitivity, specificity, and accuracy of FDG-PET in this tumor have relevant impacts on treatment [35]. Using this approach, we therefore concluded that ES cells develop a compensatory response to adverse local environment that facilitates tumor progression through the simultaneous activation of mitochondrial respiration and upregulation of glycolysis. This is in contrast with the classical Warburg theory, in which the complete loss of function of mitochondria in cancer is postulated. The role of mitochondria in cancer is still controversial, however, and in many instances tumor cells have been demonstrated to carry fully functional mitochondria [36], possibly due to the ability of cancer cells to recycle these organelles [37].

Interestingly, several ES cell lines are null for p53, possibly because the EWS-FLI1 chimeric protein can directly and indirectly interfere with p53 activity [38,39]. The inhibition, loss and/or mutation of p53, one of the most common events in tumorigenesis, results in a decreased oxygen consumption and increased glycolysis [40,41], also by enhancing HIF-1α levels [42]. As a confirmation, Knowles et al. demonstrated that ES cell lines express HIF-1α [43]. In turn, HIF-1α may induce EWS-FLI1 expression in a time-dependent manner [18,19]. Notably, A-673 and SK-N-MC show higher levels of HIF1α activation when compared to RD-ES and SK-ES-1 cell lines [43]. An excessive glycolytic activity in tumors can also be a consequence of microenvironmental alterations. In fact, cancer cells are induced to produce large amounts of metabolic acid generated by glycolysis, glucose utilization, and lactate production. To prevent acidity-induced apoptosis, tumor cells are forced to enhance proton efflux, leading to a significant decrease of pH in the extracellular environment [6–9]. On the other side, both human and animal tumor cells have a slightly alkaline pHi (pH 7.1-7.2) [44,45], suggesting that, despite lower than normal levels of pHe, cancer cells are capable to effectively reduce the excess of protons in the cytoplasm by active transport across the plasma membrane and storage within the lysosomal compartment. Lysosomes and lysosome-related organelles constitute a system of acidic compartments that interconnect the inside of the cell with the extracellular space via secretory and endocytic pathways. We verified the extension of the lysosomal compartment and activity in ES cells, and compared ES cells with hFG. In this paper, we used a primary culture of human fibroblasts as a control, also with the aim to demonstrate the selectiveness and effectiveness of the suggested targeting in the ES cells with respect to normal cells. Lysosomes and lysosome-related organelles were rather scanty in all ES cell lines, in sharp contrast to hFG. The observed presence of autolysosomes in ES cells further supports the hypothesis of a survival mechanism under acidic stress, as already demonstrated in other cancers [46]. In fact, even if ES cells have only a few lysosomes, the cytotoxic effect of autophagy inhibitor bafilomycin A1 is very high, especially under acidic conditions. Of note, BF-1 treatment was completely ineffective in normal human cells, also at pH 6.5. Although the level of specificity is still controversial, the main target of BF-1 is the proton pump V-ATPase. Thus, we wondered if V-ATPase could represent an effective target for the treatment of ES. V-ATPase is the major electrogenic pump of vacuolar membranes, and is crucial to establish and maintain intracellular pH gradients across specialized organelle membranes, including the trans-Golgi network, secretory granules, endosomes, and lysosomes [47]. V-ATPase has recently gained great attention in cancer, especially with regard to its role in microenvironment acidification and in metastasis [10,47]. Interestingly, among the many mechanisms that regulate the tumor microenvironment, V-ATPases are especially valuable because they can be blocked by proton pump inhibitors [48,49]. First, we looked at the V-ATPase expression and localization. V-ATPase was constantly expressed in ES cells and at the highest level both for V_0c and V_1B2 subunits in SK-N-MC, the ES cell line with the highest GAPDH expression and with the highest susceptibility to the BF-1 treatment. Notably, the signal for V-ATPase in ES cells was localized inside the cell and on the cell membrane. The membrane expression of V-ATPase is possibly due to improper sorting of normal cellular components and was proven to be functional also in other tumors [10]. Immunohistochemical analysis in breast cancer cells has revealed a higher plasmalemmal V-ATPase in highly metastatic cells compared to low metastatic cells [50,51]. Accordingly, our data suggest that V-ATPase on the membrane of ES cells is an additional factor that possibly contributes to the formation of metastases [52]. V-ATPase is usually recycled from the plasma membrane for the formation of endosomes that fuse with vesicles with hydrolytic enzymes derived from the Golgi apparatus to generate new lysosomes. Accordingly, in non permeabilized cells, we also observed the presence of V-ATPase localization in clusters closed to the plasma membrane and possibly associated with the invagination of the membrane to form endosomes. In agreement with results obtained with the level of expression of V-ATPase, we found the highest acidification rate in SK-N-MC cells. Based on our findings, glycolytic ES cells have a strong proton secretion activity that contribute to form an acidic microenvironment and that is directly related to V-ATPase expression. The low pHe has been repeatedly implicated as playing a key role both in cell transformation and in the active progression and maintenance of the neoplastic process [48]. We then verified the consequence of the acidification activity exerted by the V-ATPase activity in ES cells. Adachi and Tannock induced intratumoral acidification in an in vivo cancer model by using the vasodilating drug captopril, and simultaneously obtained a significant delay in tumor growth [53]. Consistent with these in vivo data, we found that under acidic (6.5) in vitro pH conditions, the number of ES cells is significantly decreased. However, the number of apoptotic cell is not affected whereas the percentage of cells in G0–G1 phase is increased. Thus, the reduction in cell number is a consequence of a delay of the cell cycle rather than of a cytotoxic effect of the acidic pHe. On the other hand, the ability to degrade gelatin and bone collagen and the clonogenic efficiency is significantly increased. An increased invasion ability under acidic conditions is a well-known feature of tumor cells that is due to an increase of matrix metalloproteinase [48,54]. In ES, the observed collagen and gelatin degradation is possibly a consequence of the secretion of MMP-9 [55–57]. In this tumor, the increased invasive capacity and the enhanced cloning efficiency has been previously

demonstrated also under hypoxia [18], which, however, directly concurs to the acidification of tumor microenvironment. Consequently, in ES cells the ability to survive and to invade the surrounding tissues under acidic conditions is increased, possibly through the activation of V-ATPase.

In an effort to consider V-ATPase as a candidate therapeutic target for ES, we focused on the inhibitory effect of this proton pump on tumor growth. First, to directly correlate the cell number inhibition with impairment of V-ATPase expression we used a more specific targeting technique than BF-1 treatment. siRNA silencing strongly affected V_0c mRNA expression and resulted in a significant reduction of the number of ES cells. We chose the V_0c subunit because its inhibition was very effective to impair growth and chemoresistance also in other tumors [13,29]. Moreover, the V_0c subunit is the target of the V-ATPase inhibitor BF-1 [58] that already showed to be effective in ES cells, as described above. Secondly, we used OME which is known to block V-ATPase through the binding to the V_1A subunit [59]. Among the different proton transporter/ion inhibitors, OME and other related drugs have sparked great interest in cancer [48,60]. Two important attractive features of these agents are that they require acidic conditions to be converted into the active form, thus providing the possibility of tumor-specific selection, and that their use in long-term therapy produces only limited side effects [61]. Proton pump inhibitors have been previously used in sarcoma and bone tumor patients at low dosage, and only to prevent gastric lesions as a side effect of the treatment with conventional drugs. Therefore, proton pump inhibitors have been never described and published in sarcomas as an anti-cancer therapy. We obtained a significant reduction of the number of cells that survived under low pHe with either siRNA, or OME. Moreover, we observed a dose-dependent effect of OME treatment.

In summary, in this study we focused on the consequences of the metabolic alterations of ES. We demonstrated that activation of V-ATPase is a necessary survival mechanism in an acidic microenvironment and that V-ATPase should be considered as a promising therapeutic target.

5. Conclusions

The peculiar metabolic derangements, including the acidification of extracellular microenvironment, have not been considered so far as a basis for novel therapeutic targets in ES. In this study, we demonstrate that ES cells strongly acidify the medium and can survive under acidic pHe through the activity of a plasmalemmal V-ATPase. Moreover, we also show that the survival of ES can be effectively impaired by anti-V-ATPase strategies. In conclusion, although results from this study warrant further investigations also in an in vivo model of this cancer, this paper endorses the use of anti-V-ATPase agents, such as proton-pump inhibitors, for the treatment of ES.

Acknowledgement

Grant support: Ministry of Health (n. of grant: RBAP10447J_004 to N. Baldini), Italian Association for Cancer Research (n. of grant: 11426 to N. Baldini).

References

[1] R.A. Gatenby, R.J. Gillies, A microenvironmental model of carcinogenesis, Nat. Rev. Cancer 8 (2008) 56–61.
[2] D. Hanahan, R.A. Weinberg, Hallmarks of cancer: the next generation, Cell 144 (2011) 646–674.
[3] O. Warburg, On the origin of cancer cells, Science 123 (1956) 309–314.
[4] K.L. Bennewith, R.E. Durand, Quantifying transient hypoxia in human tumor xenografts by flow cytometry, Cancer Res. 64 (2004) 6183–6189.
[5] J. Czernin, M.E. Phelps, Positron emission tomography scanning: current and future applications, Annu. Rev. Med. 53 (2002) 89–112.
[6] K. Engin, D.B. Leeper, J.R. Cater, A.J. Thistlethwaite, L. Tupchong, J.D. McFarlane, Extracellular pH distribution in human tumours, Int. J. Hyperthermia 11 (1995) 211–216.
[7] F. Timeus, E. Ricotti, N. Crescenzio, E. Garelli, A. Doria, M. Spinelli, U. Ramenghi, G. Basso, Flt-3 and its ligand are expressed in neural crest-derived tumors and promote survival and proliferation of their cell lines, Lab. Invest. 81 (2001) 1025–1037.
[8] T. Morita, Low pH leads to sister-chromatid exchanges and chromosomal aberrations, and its clastogenicity is S-dependent, Mutat. Res. 334 (1995) 301–308.
[9] X. Zhang, Y. Lin, R.J. Gillies, Tumor pH and its measurement, J. Nucl. Med. 51 (2010) 1167–1170.
[10] H. Izumi, T. Torigoe, H. Ishiguchi, H. Uramoto, Y. Yoshida, M. Tanabe, T. Ise, T. Murakami, T. Yoshida, M. Nomoto, K. Kohno, Cellular pH regulators: potentially promising molecular targets for cancer chemotherapy, Cancer Treat. Rev. 29 (2003) 541–549;
R. Martinez-Zaguilan, R.M. Lynch, G.M. Martinez, R.J. Gillies, Vacuolar-type H(+)-ATPases are functionally expressed in plasma membranes of human tumor cells, Am. J. Physiol. 265 (1993) C1015–C1029.
[11] S.R. Sennoune, R. Martinez-Zaguilan, Vacuolar H(+)-ATPase signaling pathway in cancer, Curr. Protein Pept. Sci. 13 (2012) 152–163.
[12] V. Michel, Y. Licon-Munoz, K. Trujillo, M. Bisoffi, K.J. Parra, Inhibitors of vacuolar ATPase proton pumps inhibit human prostate cancer cell invasion and prostate-specific antigen expression and secretion, Int. J. Cancer 132 (2013) E1–E10.
[13] X. Lu, W. Qin, J. Li, N. Tan, D. Pan, H. Zhang, L. Xie, G. Yao, H. Shu, M. Yao, D. Wan, J. Gu, S. Yang, The growth and metastasis of human hepatocellular carcinoma xenografts are inhibited by small interfering RNA targeting to the subunit ATP6L of proton pump, Cancer Res. 65 (2005) 6843–6849.
[14] C. Chung, C.C. Mader, J.C. Schmitz, J. Atladottir, P. Fitchev, M.L. Cornwell, A.J. Koleske, S.E. Crawford, F. Gorelick, The vacuolar-ATPase modulates matrix metalloproteinase isoforms in human pancreatic cancer, Lab. Invest. 91 (2011) 732–743.
[15] K.C. Jefferies, D.J. Cipriano, M. Forgac, Function, structure and regulation of the vacuolar (H+)-ATPases, Arch. Biochem. Biophys. 476 (2008) 33–42.
[16] J. Potratz, U. Dirksen, H. Jürgens, A. Craft, Ewing sarcoma: clinical state-of-the-art, Pediatr. Hematol. Oncol. 29 (2012) 1–11.
[17] C. Mackintosh, J. Madoz-Gúrpide, J.L. Ordóñez, D. Osuna, D. Herrero-Martín, The molecular pathogenesis of Ewing's sarcoma, Cancer Biol. Ther. 9 (2010) 655–667.
[18] D.N. Aryee, S. Niedan, M. Kauer, R. Schwentner, I.M. Bennani-Baiti, J. Ban, K. Muehlbacher, M. Kreppel, R.L. Walker, P. Meltzer, C. Poremba, R. Kofler, H. Kovar, Hypoxia modulates EWS-FLI1 transcriptional signature and enhances the malignant properties of Ewing's sarcoma cells in vitro, Cancer Res. 70 (2010) 4015–4023.
[19] W. Zeng, R. Wan, Y. Zheng, S.R. Singh, Y. Wei, Hypoxia, stem cells and bone tumor, Cancer Lett. 313 (2011) 129–136.
[20] G.L. Semenza, Hypoxia-inducible factor 1 (HIF-1) pathway, Sci. STKE 2007 (2007) cm8.
[21] M.C. Brahimi-Horn, G. Bellot, J. Pouyssegur, Hypoxia and energetic tumour metabolism, Curr. Opin. Genet. Dev. 21 (2011) 67–72.
[22] A. Greenspan, G. Jundt, W. Remagen, Differential diagnosis in orthopaedic oncology, second ed. Lippincott Williams and Wilkins, Philadelphia, PA, 2007.
[23] L. Checchi, G. Ciapetti, G. Monaco, G. Ori, The effects of nicotine and age on replication and viability of human gingival fibroblasts in vitro, J. Clin. Periodontol. 26 (1999) 636–642.
[24] T.T. Yang, P. Sinai, S.R. Kain, An acidic phosphatase assay for quantifying the growth of adherent and nonadherent cells, Anal. Biochem. 241 (1996) 103–108.
[25] M.W. Pfaffl, A new mathematical model for relative quantification in real-time RT-PCR, Nucleic Acids Res. 29 (2001) e45.
[26] J.M. Cuezva, G. Chen, A.M. Alonso, A. Isidoro, D.E. Misek, S.M. Hanash, D.G. Beer, The bioenergetic signature of lung adenocarcinomas is a molecular marker of cancer diagnosis and prognosis, Carcinogenesis 27 (2004) 1157–1163.
[27] J.M. Cuezva, M. Krajewska, M.L. de Heredia, S. Krajewski, G. Santamaría, H. Kim, J.M. Zapata, H. Marusawa, M. Chamorro, J.C. Reed, The bioenergetic signature of cancer: a marker of tumor progression, Cancer Res. 62 (2002) 6674–6681.
[28] J. Zhang, E. Nuebel, D.R. Wisidagama, K. Setoguchi, J.S. Hong, C.M. Van Horn, S.S. Imam, L. Vergnes, C.S. Malone, C.M. Koehler, M.A. Teitell, Measuring energy metabolism in cultured cells, including human pluripotent stem cells and differentiated cells, Nat. Protoc. 7 (2012) 1068–1085.
[29] H. You, J. Jin, H. Shu, B. Yu, A. De Milito, F. Lozupone, Y. Deng, N. Tang, G. Yao, S. Fais, J. Gu, W. Qin, Small interfering RNA targeting the subunit ATP6L of proton pump V-ATPase overcomes chemoresistance of breast cancer cells, Cancer Lett. 280 (2009) 110–119.
[30] J.H. Lim, J.W. Park, S.J. Kim, M.S. Kim, S.K. Park, R.S. Johnson, Y.S. Chun, ATP6V0C competes with Von Hippel-Lindau protein in hypoxia-inducible factor 1α (HIF-1α) binding and mediates HIF-1α expression by bafilomycin A1, Mol. Pharmacol. 71 (2007) 942–948.
[31] E.J. Bowman, B.J. Bowman, V-ATPases as drug targets, J. Bioenerg. Biomembr. 37 (2005) 431–435.
[32] C. Eng, M. Kiuru, M.J. Fernandez, L.A. Aaltonen, A role for mitochondrial enzymes in inherited neoplasia and beyond, Nat. Rev. Cancer 3 (2003) 193–202.
[33] M.E. Perry, C.V. Dang, D. Hockenbery, U. Moll, Highlights of the National Cancer Institute Workshop on mitochondrial function and cancer, Cancer Res. 64 (2004) 7640–7644.
[34] E. Seppet, M. Gruno, A. Peetsalu, Z. Gizatullina, H.P. Nguyen, S. Vielhaber, M.H. Wussling, S. Trumbeckaite, O. Arandarcikaite, D. Jerzembeck, M. Sonnabend, K. Jegorov, S. Zierz, F. Striggow, F.N. Gellerich, Mitochondria and energetic depression in cell pathophysiology, Int. J. Mol. Sci. 10 (2009) 2252–2303.
[35] G. Treglia, M. Salsano, A. Stefanelli, M.V. Mattoli, A. Giordano, L. Bonomo, Diagnostic accuracy of (1)(8)F-FDG-PET and PET/CT in patients with Ewing sarcoma family tumours: a systematic review and a meta-analysis, Skeletal Radiol. 41 (2012) 249–256.
[36] F. Weinberg, N.S. Chandel, Mitochondrial metabolism and cancer, Ann. N. Y. Acad. Sci. 1177 (2009) 66–73.

[37] S. Bonnet, S.L. Archer, J. Allalunis-Turner, A. Haromy, C. Beaulieu, R. Thompson, C.T. Lee, G.D. Lopaschuk, L. Puttagunta, G. Harry, K. Hashimoto, C.J. Porter, M.A. Andrade, B. Thebaud, E.D. Michelakis, A mitochondria-K+ channel axis is suppressed in cancer and its normalization promotes apoptosis and inhibits cancer growth, Cancer Cell 11 (2007) 37–51.
[38] J. Ban, I.M. Bennani-Baiti, M. Kauer, K.L. Schaefer, C. Poremba, G. Jug, R. Schwentner, O. Smrzka, K. Muehlbacher, D.N. Aryee, H. Kovar, EWS-FLI1 suppresses NOTCH-activated p53 in Ewing's sarcoma, Cancer Res. 68 (2008) 7100–7109.
[39] P.M. Neilsen, K.I. Pishas, D.F. Callen, D.M. Thomas, Targeting the p53 pathway in Ewing sarcoma, Sarcoma 2011 (2011) 746939.
[40] E. Madan, R. Gogna, M. Bhatt, U. Pati, P. Kuppusamy, A.A. Mahdi, Regulation of glucose metabolism by p53: emerging new roles for the tumor suppressor, Oncotarget 2 (2011) 948–957.
[41] X.D. Zhang, Z.H. Qin, J. Wang, The role of p53 in cell metabolism, Acta Pharmacol. Sin. 31 (2010) 1208–1212.
[42] R. Ravi, B. Mookerjee, Z.M. Bhujwalla, C.H. Sutter, D. Artemov, Q. Zeng, L.E. Dillehay, A. Madan, G.L. Semenza, A. Bedi, Regulation of tumor angiogenesis by p53-induced degradation of hypoxia-inducible factor 1alpha, Genes Dev. 14 (2000) 34–44.
[43] H.J. Knowles, K.L. Schaefer, U. Dirksen, N.A. Athanasou, Hypoxia and hypoglycaemia in Ewing's sarcoma and osteosarcoma: regulation and phenotypic effects of Hypoxia-Inducible Factor, BMC Cancer 10 (2010) 372.
[44] I.F. Tannock, D. Rotin, Acid pH in tumors and its potential for therapeutic exploitation, Cancer Res. 49 (1989) 4373–4384.
[45] L.E. Gerweck, K. Seetharaman, Cellular pH gradient in tumor versus normal tissue: potential exploitation for the treatment of cancer, Cancer Res. 56 (1996) 1194–1198.
[46] M.L. Marino ML, P. Pellegrini, G. Di Lernia, M. Djavaheri-Mergny, S. Brnjic, X. Zhang, M. Hägg, S. Linder, S. Fais, P. Codogno, A. De Milito, Autophagy is a protective mechanism for human melanoma cells under acidic stress, J. Biol. Chem. 287 (2012) 30664–30676.
[47] T. Nishi, M. Forgac, The vacuolar (H+)-ATPases—nature's most versatile proton pumps, Nat. Rev. Mol. Cell Biol. 3 (2002) 94–103.
[48] S. Fais, A. De Milito, H. You, W. Qin, Targeting vacuolar H+-ATPases as a new strategy against cancer, Cancer Res. 67 (2007) 10627–10630.
[49] A. De Milito, R. Canese, M.L. Marino, M. Borghi, M. Iero, A. Villa, G. Venturi, F. Lozupone, E. Iessi, M. Logozzi, P. Della Mina, M. Santinami, M. Rodolfo, F. Podo, L. Rivoltini, S. Fais, pH-dependent antitumor activity of proton pump inhibitors against human melanoma is mediated by inhibition of tumor acidity, Int. J. Cancer 127 (2010) 207–219.
[50] S.R. Sennoune, K. Bakunts, G.M. Martinez, J.L. Chua-Tuan, Y. Kebir, M.N. Attaya, R. Martinez-Zaguilan, Vacuolar H+-ATPase in human breast cancer cells with distinct metastatic potential: distribution and functional activity, Am. J. Physiol. Cell Physiol. 286 (2004) C1443–C1452.
[51] S.R. Sennoune, D. Luo, R. Martinez-Zaguilan, Plasmalemmal vacuolar-type H+-ATPase in cancer biology, Cell Biochem. Biophys. 40 (2004) 185–206.
[52] N.J. Balamuth, R.B. Womer, Ewing's sarcoma, Lancet Oncol. 11 (2010) 184–192.
[53] E. Adachi, I.F. Tannock, The effects of vasodilating drugs on pH in tumors, Oncol. Res. 11 (1999) 179–185.
[54] Y. Kato, Y. Nakayama, M. Umeda, K. Miyazaki, Induction of 103-kDa gelatinase/type IV collagenase by acidic culture conditions in mouse metastatic melanoma cell lines, J. Biol. Chem. 267 (1992) 11424–11430.
[55] H. Yabe, M. Fukuma, F. Urano, K. Yoshida, S. Kato, Y. Toyama, J. Hata, A. Umezawa, Lack of matrix metalloproteinase (MMP)-1 and -3 expression in Ewing sarcoma may be due to loss of accessibility of the MMP regulatory element to the specific fusion protein in vivo, Biochem. Biophys. Res. Commun. 293 (2002) 61–71.
[56] J. Sanceau, S. Truchet, B. Bauvois, Matrix metalloproteinase-9 silencing by RNA interference triggers the migratory-adhesive switch in Ewing's sarcoma cells, J. Biol. Chem. 278 (2003) 36537–36546.
[57] S. Benini, M. Zuntini, M.C. Manara, P. Cohen, G. Nicoletti, P. Nanni, Y. Oh, P. Picci, K. Scotlandi, Insulin-like growth factor binding protein 3 as an anticancer molecule in Ewing's sarcoma, Int. J. Cancer 119 (2006) 1039–1046.
[58] E.J. Bowman, L.A. Graham, T.H. Stevens, B.J. Bowman, The bafilomycin/concanamycin binding site in subunit c of the V-ATPases from *Neurospora crassa* and *Saccharomyces cerevisiae*, J. Biol. Chem. 279 (2004) 33131–33138.
[59] Y. Moriyama, V. Patel, I. Ueda, M. Futai, Evidence for a common binding site for omeprazole and N-ethylmaleimide in subunit A of chromaffin granule vacuolar-type H(+)-ATPase, Biochem. Biophys. Res. Commun. 196 (1993) 699–706.
[60] A. De Milito, M.L. Marino, S. Fais, A rationale for the use of proton pump inhibitors as antineoplastic agents, Curr. Pharm. Des. 18 (2012) 1395–1406.
[61] T.B. Nealis, C.W. Howden, Is there a dark side to long-term proton pump inhibitor therapy? Am. J. Ther. 15 (2008) 536–542.